Pseudo-tetragonal tungsten bronze superstructure: a combined solution of the crystal structure of $K_{6.4}(Nb,Ta)_{36.3}O_{94}$ with advanced transmission electron microscopy and neutron diffraction.

Robert Paria Sena,[a] Artem A. Babaryk,*[b,c] Sergiy Khainakov,[c] Santiago Garcia-Granda,[c] Nikolay S. Slobodyanik,[b] Gustaaf Van Tendeloo,[a] Artem M. Abakumov[a] and Joke Hadermann*[a]

[a]Electron Microscopy for Materials Research (EMAT), University of Antwerp, Groenenborgerlaan 171, B-2020, Antwerp, Belgium

[b]Faculty of Chemistry, Taras ShevchenkoNational University of Kyiv, Volodymyrska 64/13, 01601 Kyiv, Ukraine

[c]Department of Fisical and Inorganic Chemistry, Faculty of Chemistry, University of Oviedo, C/ Julian Claveria 8, 33006 Oviedo, Spain

*Corresponding author.
Tel: 00 32 653245. Fax: 00 32 032653318.
E-mail address:joke.hadermann@uantwerpen.be, babaryk@univ.kiev.ua

Abstract

The crystal structure of the $K_{6.4}Nb_{28.2}Ta_{8.1}O_{94}$ pseudo-tetragonal tungsten bronze-type oxide was determined using a combination of X-ray powder diffraction, neutron diffraction and transmission electron microscopy techniques, including electron diffraction, high angle annular dark field scanning transmission electron microscopy (HAADF-STEM),annular bright field STEM (ABF-STEM) and energy-dispersive X-ray compositional mapping (STEM-EDX). The compound crystallizes in the space group *Pbam* with unit cell parameters a = 37.468(9) Å, b = 12.493(3) Å, c = 3.95333(15) Å. The structure consists of corner

sharing $(Nb,Ta)O_6$ octahedra forming trigonal, tetragonal and pentagonal tunnels. All tetragonal tunnels are occupied by K^+ ions, while 1/3 of the pentagonal tunnels are preferentially occupied by Nb^{5+}/Ta^{5+} and 2/3 are occupied by K^+ in a regular pattern. A fractional substitution of K^+ in the pentagonal tunnels by Nb^{5+}/Ta^{5+} is suggested from the analysis of the HAADF-STEM images. Contrary to similar structures, such as $K_2Nb_8O_{21,}$ also part of the trigonal tunnels are fractionally occupied by K^+ cations.

Keywords: Potassium niobate, potassium tantalate, tetragonal tungsten bronze, TEM, $K_2Nb_8O_{21.}$

1. Introduction

Alkali or alkali earth metal niobates have been intensely investigated as dielectric materials[1], gas sensors, UV-detectors[2] and photocatalysts [3]. Among these, "$K_2Nb_8O_{21}$" attracts particular attention, because it can be obtained in many different shapes: nanoribbons[1], micro/nanowires[2-4], whiskers[2], nanorods[5], tubes[3], and nanobelts[4]. Since its first preparation in 1962[6], the crystal structure of this material has not yet been completely established. Different groups[7-9] report on the investigation of the unit cell parameters based X-ray powder diffraction or an analysis of TEM/SAED data. Roth et al.[7] suggested systematic absences consistent with *Pbam* or *Pba*2 space groups. Irle et al.[9] reduced the choice to *Pbam* only, referring to original tests on second harmonic generation (SHG) activity. Later investigations by Li et al.[10] suggest that the actual composition of "$K_2Nb_8O_{21}$" is $K_4Nb_{17}O_{45}$ based on the structure solved from crystallographic image processing of high resolution transmission electron microscopy images. However, the proposed composition $K_4Nb_{17}O_{45}$ does not satisfy the charge balance and, moreover, the space group $P2_12_12$ proposed by Li et al.[10] is not in

agreement with other findings. This calls for a more detailed investigation of this crystal structure.

In this paper we attempt to clarify the structure using a compound synthesized following the synthesis method for "$K_2Nb_8O_{21}$" described in[1], but with addition of Ta. The addition of Ta to the Nb positions will enhance the clarity of their positions when using HAADF-STEM imaging of the cation positions. We solved the crystal structure using transmission electron microscopy techniques, and based on the results of the compositional analysis and structure solution we propose the $K_{6.4}Nb_{28.2}Ta_{8.1}O_{94}$ formula. The obtained cell parameters are identical to those described in literature, but with a different distribution of the cations over the different channels.

2. Experimental section

$K_{6.4}Nb_{28.2}Ta_{8.1}O_{94}$ was synthesized via a two-step route. Initially Nb_2O_5 was mixed and ground with 18-fold excess of KCl, then the blend was gradually heated in a ceramic tray to 800 °C until it melted. After 6 hours of exposure, the muffle furnace was switched off and the melt was cooled down to room temperature. The solidified melt was leached out with deionized water until a negative probe was obtained for the presence of Cl^- anions with an $AgNO_3$ test solution. The recovered white powder was dried overnight in an oven at 60 °C. PXRD phase analysis showed the presence of KNb_3O_8 as a single entity in the product. At the second step KNb_3O_8 and Ta_2O_5 were mixed in a molar ratio 2:1, pressed into a tablet at isostatic pressure of 10^5 $N.m^{-2}$ and fired at 1000 °C in a furnace for 24 h resulting in a yellow-coloured powder.

An X-ray powder diffraction pattern was collected at room temperature on a Panalytical X'Pert Pro diffractometer, equipped with a one-dimensional PIXcel hybrid pixel technology position sensitive device detector and operating with CuKα radiation. A full pattern

decomposition procedure was developed from the powder pattern using the Le Bail method[11] (Fig. S2). In the Rietveld refinement from combined X-ray and neutron powder diffraction data, scale factor, Chebyshev polynomials up to 20th order, cell parameters, fractional atomic coordinates, isotropic displacement parameters and Lorentzian size/strain contributions according to Balzar's (Double Voight) approach[12] were used. The instrumental function was deconvoluted by the fundamental parameters approach[13] implying physical constants of the diffractometer and apertures of optical components to be known. Preferred orientation of the crystallites was modeled by spherical harmonics series expanded to 4th order in dependent terms for the *mmm* Laue class.

Energy dispersive X-ray (EDX) analysis was performed with a JEOL JSM5510 scanning electron microscope equipped with an Oxford Instruments EDX spectrometer. The EDX spectra were collected from 50 different regions, using the K-K, Nb-L and Ta-L peaks.

Samples for transmission electron microscopy (TEM) were prepared by crushing the powder, dispersing it in ethanol and depositing a few drops of the suspension on a holey carbon grid. Selected area electron diffraction (SAED) patterns were taken on a Philips CM20 microscope, and a FEI Tecnai G2 microscope both operated at 200 kV. Tilt series were made around different axes, but only the patterns of the main zones are presented here. High angle annular dark field scanning transmission electron microscopy (HAADF-STEM), annular bright field (ABF)-STEM images and EDX images were recorded with a FEI Titan G3 microscope operating at 300 kV. HAADF-STEM and ABF-STEM images were simulated using QSTEM 2.22[14]. Calculated SAED patterns were made using CrystalKit 1.9.8. Optimization of the structure model was performed using a simulated annealing algorithm minimizing the antibump and bond valence cost functions with the FOX program package[15].

Neutron diffraction data were acquired at the D2B high-resolution powder diffractometer of the Institut Laue-Langevin (Grenoble) at a wavelength of 1.594 Å, calibrated with a

$Na_2Ca_3Al_2F_{14}$ reference. The powder was put in a vanadium cylindrical sample holder with a diameter of 6.5 mm and data were collected in the 2θ angular range of 10°−156°. Experimental observations were integrated from the whole region of the curved 128-bank [3]He detector (as an averaged signal) or from the centre of the detector providing either higher intensities and higher resolution respectively. Structural refinements using Rietveld analysis were performed using combined X-ray and neutron diffraction data, using the model based on electron microscopy results. With this approach we aimed to overcome the low sensitivity of X-ray radiation to O atoms (~Z) and the inability to discriminate Nb ($b_{coherent}$ = 7.054 fm) and Ta ($b_{coherent}$ =6.91 fm) on neutron diffraction data to derive the most reliable model. Scale factor and profile-related and cell parameters were refined for each unique dataset, while fractional atomic coordinates and its isotropic thermal parameters were kept to be common for all the data. Concerning the profile-related parameter, the background was approximated by Chebyshev polynomials up to 20th order, with Lorentzian size sample contributions in Balzar's (Double Voight) formulation[12] and the instrumental function a pseudo-Voight profile as proposed by Thompson-Cox-Hastings[13]. Preferred orientation of the crystallites was modeled by spherical harmonics series expanded to 8th order independent terms for the *mmm* Laue class. Anti-bumping bond distance restraints were applied for potassium and oxygen atoms based on repulsive terms of the Leonard Jones and Born-Mayer potentials calculated while the calculations were in progress[16].

Bruker TOPAS 4.2 software was used for all refinements.

3. Results

EDX analysis showed a cation ratio K:Nb:Ta = 0.15(2):0.66(2):0.19(2). The cell parameters determined from X-ray powder diffraction (XRPD) using the Le Bail decomposition

(R_p=1.53%, wR_p=1.95%, R_{exp}=2.03%) are a = 37.4611(3) Å, b = 12.4714(1) Å, c = 3.95427(3)

Å (Fig. S2). The extinction symbol for the space group was determined using SAED, for

which tilt series were collected around different axes. Fig. 1 shows the main zones [100],

[010] and [001]. All SAED patterns could be completely indexed using the cell parameters

determined from XRPD. The reflection conditions *hkl:* no conditions*, hk0:* no conditions, *h0l:*

h=2n, h00: h=2n are clear from these patterns (and thus part of the extinction symbol, *P.a-*),

however, there is also a *0kl*: *k*=2n reflection condition, which is not so obvious. At first sight,

most [100] patterns show a *0kl:k=2n* reflection condition, but on close inspection some very

weak reflections contradicting this reflection condition can be seen on the [100] SAED

patterns. The presence of these reflections seems to indicate the absence of reflection

conditions for *0kl* and thus extinction symbol *P-a-*. However, calculated SAED patterns using

the cell parameters obtained from XRPD show that these reflections will be present also for

Pba- space groups in spite of the reflection condition *0kl:k=2n*, and that they are in fact

reflections originating from the very nearby [1$\bar{1}$0] zone. To clarify this, the calculated [100]

SAED pattern for *Pba-* has been included as Supplementary Information Fig. S1. Therefore,

the extinction symbol is *Pba-*, with possible space groups *Pbam* and *Pba2*. To decide

between these two space groups, CBED needs to be performed, however, this is impossible

for the current material due to a high amount of twinning. Therefore, *Pbam* has been selected

for the further considerations, according to the SHG investigation from Irle et al.[9].
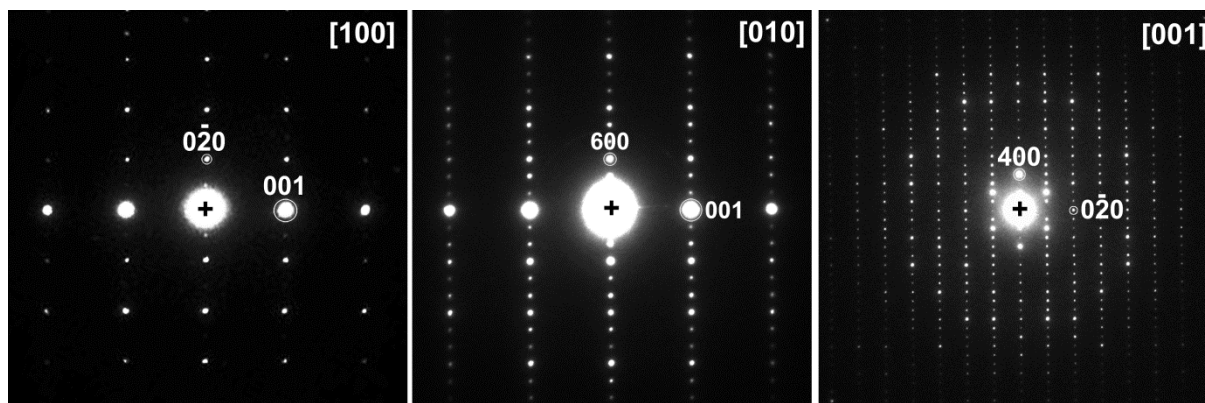
Fig. 1 SAED patterns of the main zones of $K_{6.4}Nb_{28.2}Ta_{8.1}O_{94}$.

Structure solution from precession electron diffraction or electron diffraction tomography was not possible in this case because a high amount of twinning occurs at a nanoscale; this nano-twinning was also observed in reference[17]. To determine the positions of the different atomic columns within the unit cell, we used high resolution HAADF-STEM (Fig. 2) and ABF-STEM images (Fig. 3) taken along the [001] zone axis. On HAADF-STEM images the brightness of the dots is related to the average atomic number Z along that atom column; the higher Z the brighter the dot. Therefore, in Fig. 2 the brighter dots correspond to the projected $Nb(Ta)^{5+}$(Z=41(73)) columns and less bright dots to projected K^+(Z=19) columns. In the HAADF-STEM images the oxygen columns are too faint to be visible next to the heavy atoms; they are resolved through using ABF-STEM. The size of one unit cell is marked by a white rectangle on Fig. 2. Within one unit cell, the $Nb(Ta)^{5+}$ columns form trigonal, tetragonal and pentagonal tunnels. There is a clear presence of K^+ atomic columns inside all the tetragonal tunnels. Four pentagonal tunnels are occupied by $Nb(Ta)^{5+}$ and 8 by K^+ columns. This allows building a projected model containing the coordinates of the heavier ions $Nb(Ta)^{5+}$ and K^+.
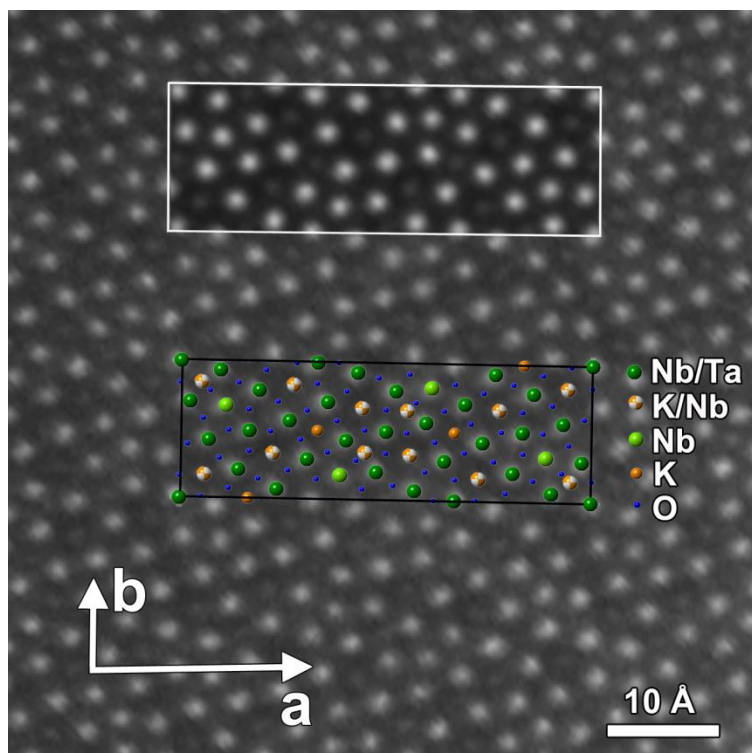
Fig. 2. HAADF-STEM image along the [001] zone of $K_{6.4}Nb_{28.2}Ta_{8.1}O_{94}$. A calculated image using the model from Table S1 is included, as well as the schematic representation of the final refined structure model.

On an ABF-STEM image such as the one shown in Fig. 3, the contrast is no longer directly related to the average Z number of a column as it is on HAADF-STEM images. However, the advantage is that also the lighter atoms, in this case the oxygen atoms, can be seen on such images. In Fig. 3, the darker dots are $Nb(Ta)^{5+}$ columns, while the fainter ones are K^+ or O^{2-}. All x and y coordinates of columns with only oxygen atoms can now also be directly estimated from the image and introduced into the model.
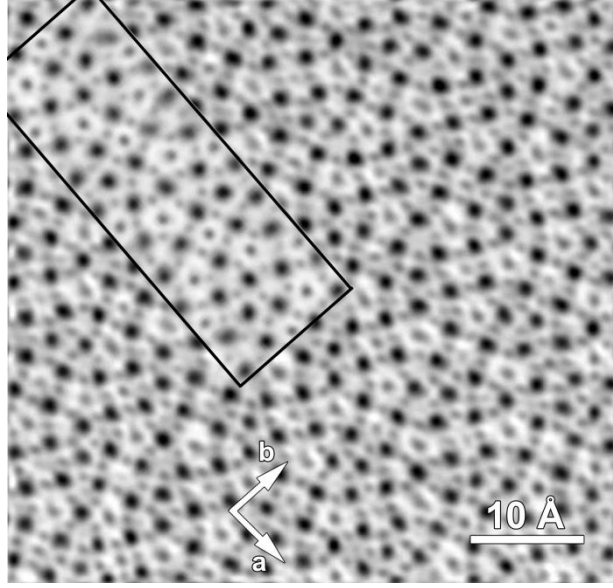
Fig. 3. ABF-STEM image (low band pass filtered) of $K_{6.4}Nb_{28.2}Ta_{8.1}O_{94}$ viewed along the [001] zone axis. A calculated ABF-STEM image using the model from TEM is shown outlined by a black rectangle.

From the combination of HAADF-STEM and ABF-STEM high resolution images, the positions of all atomic columns are now fixed, but only in projection. To complete the model with plausible z coordinates, it is sufficient to consider the space group *Pbam*: the mirror plane perpendicular to the short *c*-axis restricts the positions of the atoms to either z=0 or z=1/2. Comparing our model with other bronzes, we can find several with a similar projected structure, such as $Na_{13}Nb_{35}O_{94}$[18], $Nb_7W_{10}O_{47}$ [19] and $Nb_{16}W_{18}O_{94}$[20]. In analogy to these it is clear that the polyhedra should be completed with apical oxygen atoms at each $Nb(Ta)^{5+}$ *x-y* position, with $z_O=z_{Nb(Ta)}+1/2$, and that the relation between the z-positions of K^+ and of $Nb(Ta)^{5+}$ should be $z_K=z_{Nb(Ta)}+1/2$. The apical oxygens cannot be seen separately, since they are projected on the same dot as the $Nb(Ta)^{5+}$ positions.

Further optimization of the model is performed using a simulated annealing algorithm with antibump and bond valence cost functions. The joint population of the same crystallographic positions by the Nb and Ta cations is not an obstacle for this optimization because the R_0 and B constants in the $s = \exp((R_0 - R)/B)$ formula (s – the bond valence, R – interatomic

distance) are very close for these cations (R_0=1.911, B=0.37 for Nb^{5+}, R_0=1.92, B=0.37 for Ta^{5+} [21]). This optimized model is shown in Fig. 4. The atomic coordinates of the optimized model are given in Table S1. (Note that at this stage of the model the K^+ indicated by ° in the table are fully occupied by K^+ only and the ones indicated by * are not yet present.)
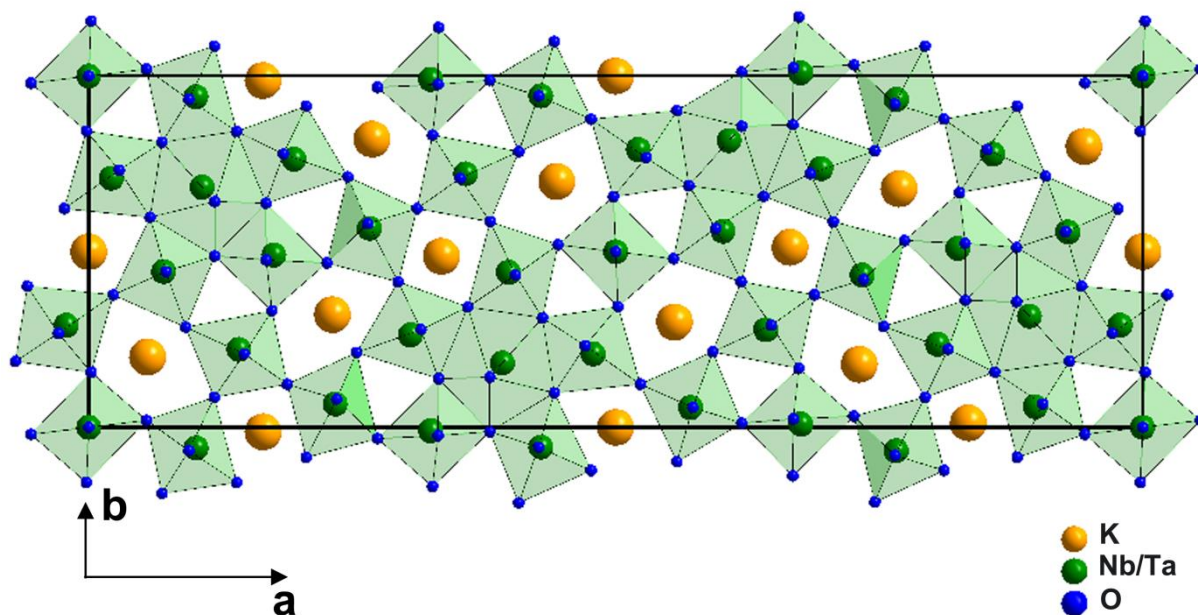

**Fig. 4.** The structure model with optimized interatomic distances, projected along [001].

The formula derived from this model, in agreement with charge balance requirements, would be $K_9(Nb,Ta)_{17}O_{47}$. However, the K:(Nb,Ta) atomic ratio of 0.346 in this formula is significantly different from the 0.176 ratio determined by EDX analysis. Therefore a more detailed inspection was made for several positions and the following observations can be made: 1) on the HAADF-STEM image the K^+ columns inside the pentagonal tunnels are not all equally bright, therefore they are not all of equal composition (Fig. 2), and 2) some of the trigonal tunnels show a clear presence of K^+ on the HAADF-STEM, ABF-STEM and STEM-EDX images (Fig. 5). On the HAADF-STEM image the K^+ columns appear as white dots in the centre of some trigonal tunnels, on ABF-STEM as black dots. On the STEM-EDX image, the EDX map of the K^+ positions (red) is overlaid onto the HAADF-STEM image. In Fig. 5 the trigonal tunnels with clear K^+ presence are indicated by circles (the clearest images for

each technique are shown, therefore the areas shown are not the same areas). Therefore we propose that the real composition is $K_{6.4}Nb_{28.2}Ta_{8.1}O_{94}$, as this is in agreement with the required charge balance and the K:(Nb,Ta) ratio is exactly as measured by EDX analysis. A fraction of the potassium atoms is located in the trigonal tunnels, divided over all available tunnels, whereas the extra $Nb(Ta)^{5+}$ ions are located in some of those pentagonal tunnels mostly filled with K^+. The positions of the K^+ in trigonal channels have been added to Table S1 and are indicated by an asterisk.

Finally, the model as-emerged from HAADF-/ABF-STEM analysis was validated by combined Rietveld refinement from X-ray and neutron powder diffraction data (Fig. 6 and Table S2, schematic model in Fig. 7). A test on concurrent occupancies over all nine Nb sites showed that they are partially filled with Ta in a Nb:Ta ratio close to 2:1, except for the pentagonal-bipyramidal Nb2(4g) position which is fully occupied by Nb. According to the procedure, all atoms of the idealized $[Nb_{26}Ta_8O_{94}]^{18-}$ skeleton were located. Further treatment of the K atoms assuming special K1 (2g) and additionally filled K5-K7 (4g) sites lead to an abnormally high isotropic displacement parameter, therefore free refinement of their atomic coordinates and occupancies was allowed. The refinement result suggests that only three of the K2-K4 have survived and K1 occupies a trigonal general (4g) position at overall improvement of the refinement. The excess of Nb atoms are distributed non-uniformly over the K1-K4 sites: K2 and K4 are statistically occupied with 28% of niobium, while the amount in K1 and K3 is none or negligible. The total amount of Nb is in good agreement with the EDX-derived bulk composition.
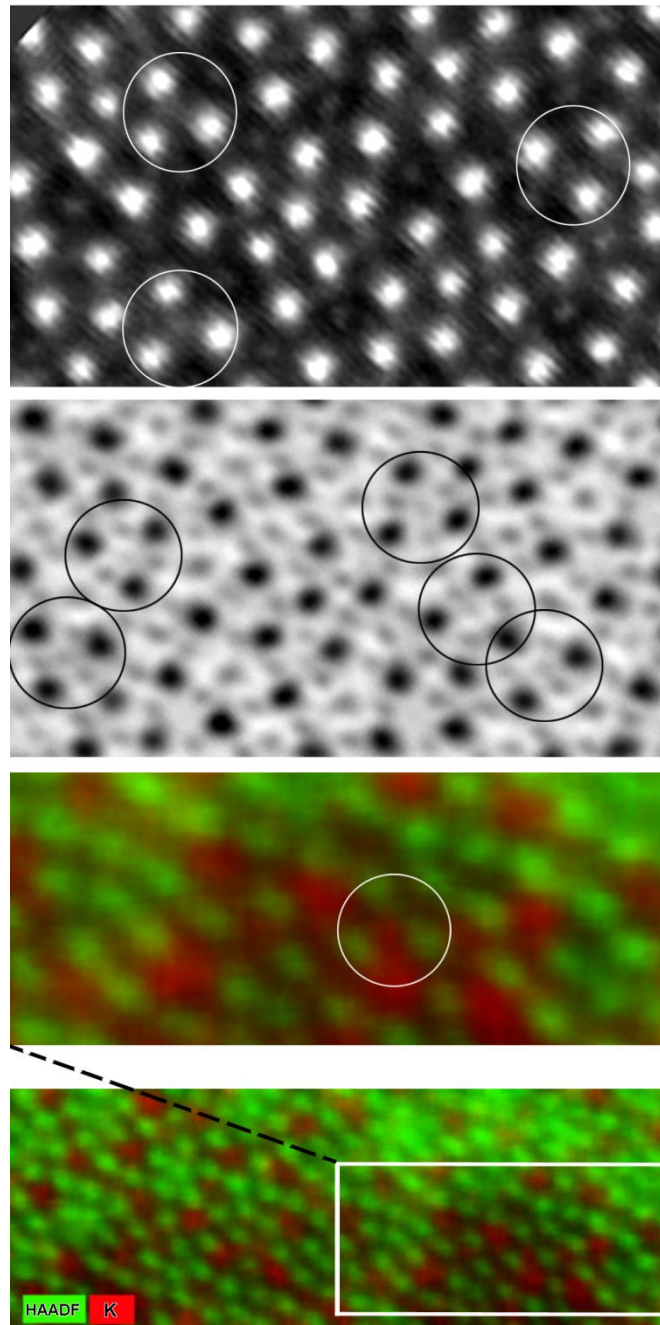
Fig. 5. Top: HAADF STEM image, second: ABF STEM image, and lowest two images: high resolution STEM-EDX map (overview and close up at same scale as the HAADF/ABF STEM images). In each image trigonal tunnels containing K^+ are indicated by circles. The top three images are shown at the same scale, but are not from the same area.
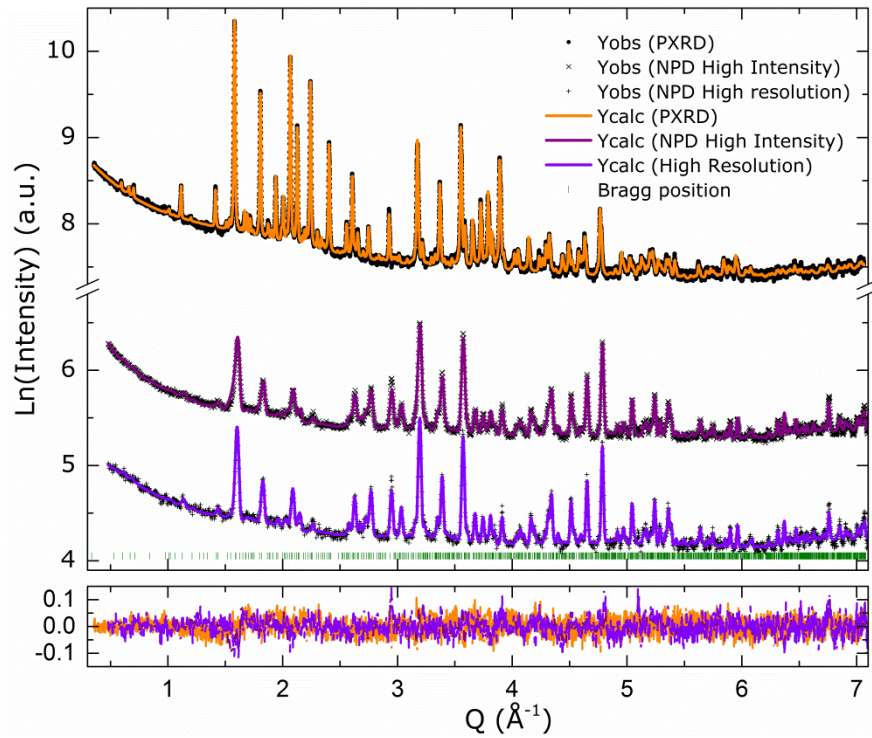
Fig. 6. Experimental (XRPD − black filled circles, NPD whole detector − ×, and the NPD center of the detector − +), calculated (superimposed orange, purple and violet solid lines) and difference (orange, purple and violet dashed lines) profiles after the combined X-ray/neutron Rietveld refinement (Rp = 1.7%, wRp = 2.6%, GoF = 1.3). Bragg positions are marked with vertical green bars.
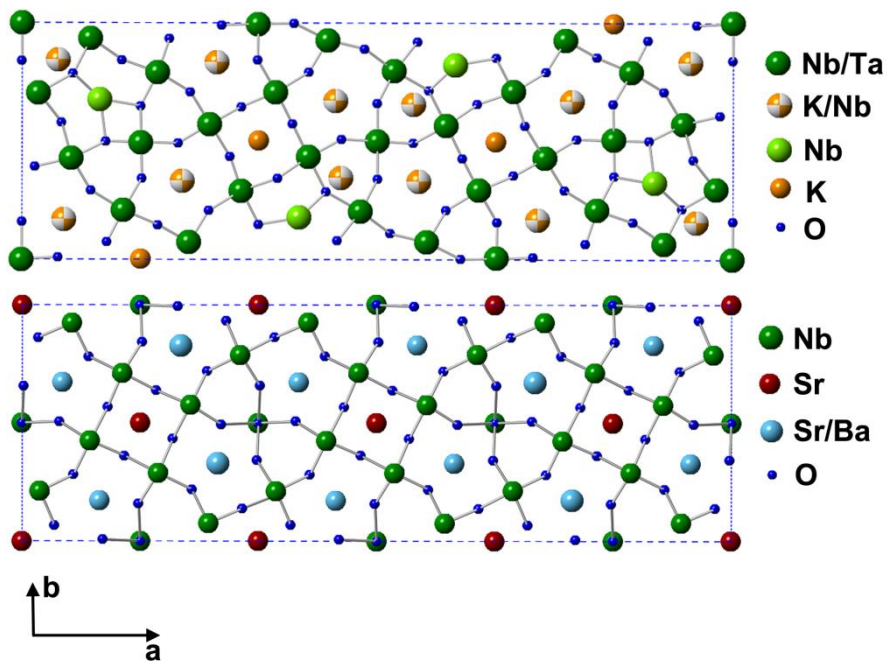
Fig. 7. Projection of the models along [001] of (top) $K_{6.4}Nb_{28.2}Ta_{8.1}O_{94}$ based on TEM and refined from combined X-ray/neutron powder diffraction data and (bottom) $Ba_{0.39}Sr_{0.61}Nb_2O_6$ (transformed to *Pba*2 for ease of comparison).

4. Discussion

As to the tetragonal tungsten bronze (TTB) domain, Roth et al.[7] indicated a narrow concentration region of $80.0 < x(Nb_2O_5) < 84.3$ mol. % and $77.8 < x(Ta_2O_5) < 81.6$ mol. % at the pseudo-binary phase diagrams Nb_2O_5-$KNbO_3$ and Ta_2O_5-$KTaO_3$ at 1000 °C. The total amount of M_2O_5 content (e.g., total mol. % of Nb_2O_5 and Ta_2O_5) for the currently reported phase is about 85%, which falls just outside the quantitative limits of the TTB phase field. Lundger and Sundberg[17] have made an attempt to explore the stoichiometric composition KNb_7O_{18} (12.5 mol. % of K_2O and 87.5 mol. % of Nb_2O_5) indexing its powder diffraction pattern only on the main reflections in the conventional TTB cell metrics ($a = b \sim 12.49$ Å, $c \sim 3.96$ Å), but with the remark that superstructure reflections were observed. Complementary HRTEM observations were interpreted as a microstructure of the TTB type, intergrown with H-Nb_2O_5 and $KNb_{13}O_{33}$ inclusions, thus giving rise to a compositional inhomogeneity. A phase with similar cell parameters was designed by Irle et al.[9] to exist in the range $79.2 < x(Nb_2O_5) < 81.6$ mol. %.

The structure of $K_{6.4}Nb_{28.2}Ta_{8.1}O_{94}$ solved in this paper is very similar to that of $K_4Nb_{17}O_{45}$ as solved by Li et al.[10], however in our case there is a definite presence of K^+ ions in the tetragonal tunnels and in the trigonal tunnels, plus the placement of about/less than one $Nb(Ta)^{5+}$ per unit cell in a K^+ position in a pentagonal tunnel, making those occupied by a combination of K^+ and $Nb(Ta)^{5+}$ in a ratio close to 3:1. In the model by Li et al.[10] the trigonal and tetragonal tunnels were left empty. Our model resembles that of $Na_{13}Nb_{35}O_{94}$, where the tetragonal tunnels are occupied by Na^+, and several pentagonal tunnels are occupied by a

combination of sodium and niobium in a ratio 3:1, however there the trigonal tunnels are empty. Furthermore, the space group derived for our compound from SAED is *Pbam* (corresponding to the one proposed by Roth et al.[7] for "$K_2Nb_8O_{21}$", while Li et al.[10] and also Teng et al.[22] solved their structure in *P2$_1$2$_1$2*. In our case the clear reflection condition *h0l:h=2n* definitely rules out the possibility of *P2$_1$2$_1$2*.

Data mining for a close structured candidate lead to a match with $Ba_{0.39}Sr_{0.61}Nb_2O_6$ (space group *P4bm*, *a* = 12.488 Å, *c* = 3.949 Å, *c/a* = 0.3162)[23]. For the sake of comparison, we transformed the structure to the maximal subgroup *Pba2* with the (3 0 0, 0 1 0, 0 0 1) translation matrix[23] (Fig. 7). Apart from additional filling of the trigonal channels with K atoms as mentioned before, it is worth to notice that the pentagonal channels host either K or Nb in the present case, whereas for the reference structure these are occupied by a Sr/Ba mixture.

To explain the present observations, we employed the charge distribution method[25]. Using this method, the ratio *q/Q* (formal oxidation number/calculated charge) for K2/Nb2 and K4/Nb4 are 2.134/2.028 and 1.69/1.753. The calculated charge was obtained using the "Charge Distribution Method"(CHARDI).[25] The ratios are close to 1, suggesting that the established partial occupancies are correct. Remarkably, the absolute values of *q* and *Q* are between the formal charges (oxidation numbers) of K^+ and Nb^{5+}, but also close to the formal charges of Sr^{2+} and Ba^{2+} that are frequently found in TTB structures[26]. It likely indicates that the effective charge on the Ta atoms might be comparable to that on the Ba atoms, permitting concurrent distributions on charge compensating positions[27], but such assumption must be confirmed by theoretical calculations, which are not accessible for the present case due to multiple statistical disorder.

Even though there is Ta in our compound, the identical NbO_6 framework suggests it would be worthwhile to reinvestigate the pure niobate analog using the current advanced TEM

techniques, to clarify the position of the K^+ ions in the different tunnels also for the pure Nb-compound. It is noteworthy that in $K_xLi_yWO_3$ the authors also concluded that the trigonal channels were occupied, albeit with the Li^+ cations.[28]

Aside from the similar bronzes mentioned in the results section, there are other bronzes in literature with very similar parameters, but for which neither the space group nor the structure has so far been solved, such as $Nb_8W_9O_{47}$ ($a = 36.69$ Å, $b = 12.19$ Å, $c = 3.945$ Å)[29] and $Pb_{0.065}Nb_{0.935}O_{2.17}F_{0.47}$($a = 37.11$ Å, $b = 12.433$ Å, $c = 3.947$ Å)[30]. Possibly they are isostructural to $K_{6.4}Nb_{28.2}Ta_{8.1}O_{94.}$

5. Conclusions

The compound $K_{6.4}Nb_{28.2}Ta_{8.1}O_{94}$ was synthesized via two-step solid state route and its structure was determined using a combination of X-ray, neutron diffraction and imaging TEM techniques. The space group *Pbam* with unit cell parameters $a = 37.468(9)$ Å, $b = 12.493(3)$ Å, $c = 3.95333(15)$ Å is established and, contrary to previous models for related compounds such as $K_2Nb_8O_{21}$, a clear presence is observed of K^+ in the trigonal and tetragonal tunnels. Arguments are given that also point to a possible different composition and cation distribution for the related $K_2Nb_8O_{21}$ than reported in literature.

Supplementary Information

Calculated SAED pattern of the [100] zone, Le Bail decomposition of PXRD profile, crystal data for $K_{6.4}Nb_{28.2}Ta_{8.1}O_{94}$ derived from transmission electron microscopy data and from the Rietveld refinement against combined X ray powder and neutron powder diffraction data.

Acknowledgements

References

[1] X. Cheng-Yan, Z. Liang, Y. Li, H. Kai, S. Wen-Zhu and Q. Lu-Chang, *Ceramics International*, 2008, **34**, 435.

[2] C. Y. Xu, L. Zhen, J. T. Jiang, C. S. Lao and L. Yang, *Ceramics International*, 2009, **35**, 3021.

[3] K. Teshima, Y. Niina, K. Yubuta, T. Nakazawa, T. Suzuki, T. Shishido, N. Ishizawa, and S. Oishi, *Japanese Journal of Applied Physics*, 2008, **47**, 629.

[4] B. Yu, B. Cao, H. Cao, X. Zhang, D. Chen, J. Qu and H. Niu, *Nanotechnology*, 2013, **24**, 085704.

[5] X. Cheng-Yan, Z. Liang, Y. Rusen and W. Zhong Lin, *J. Am. Chem. Soc.*, 2007, **129**, 15444.

[6] J. E. Guerchais, *Bull. Soc. Chim. France*, 1962, **1**, 103.

[7] R. S. Roth, H. S. Parker, W. S. Brower and D. B. Minor, *NASA Techn. Report CR*,1974, 134599.

[8] P. Appendino, *Ann. Chim. (Rome)*, 1973, **63**, 547.

[9] E. Irle, R. Blachnik and B. Gather, *Thermochimica Acta*, 1991, **179**, 157.

[10] F. H. Li, *Journal of Microscopy*, 1998, **190**, 249.

[11] A. Le Bail, H. Duroy and J. L. Fourquet, *Mat. Res. Bull.*, 1988, **23**, 447.

[12] D. Balzar, R. L. Snyder, H. J. Bunge and J. Fiala, *Microstructure Analysis from Diffraction*, Oxford University Press/International Union of Crystallography, 1999.

[13] P. Thompson, D. E. Cox and J. B. Hastings, *J. Appl. Cryst.*, 1987, **20**, 79.

[14] C. Koch, Ph.D. thesis "Determination of core structure periodicity and point defect density along dislocations", Arizona State University, 2002.

[15] V. Favre-Nicolin and R. Cerny, *J. Appl. Cryst.*, 2002, **35**, 734.

[16] A. A. Coelho and R. W. Cheary, *Computer Physics Communications*, 1997, **104**, 15.

[17] M. Lundberg and M. Sundberg, *J. Solid State Chem.*, 1986, **63**, 216.

[18] D. C. Craig and N. C. Stephenson, *J. Solid State Chem.*, 1971, **3**, 89.

[19] F. Krumeich, M. Worle and A. Hussain, *J. Solid State Chem.*, 2000, **149**, 428.

[20] A. W. Sleight, *Acta Chemica Scandinavica*, 1966, **20**, 1102.

[21] Brown and Altermatt, *Acta Cryst. B*, 1985, **41**, 244.

[22] C. M. Teng, F. H. Li, D. Y. Yang and Q. Z. Wu, *J. Chin. Ceram. Soc.*, 1986, **4**, 484.

[23] J. Schefer, D. Schaniel, V. Petricek, T. Woike , A. Cousson and M. Woehlecke, *Z. Kristallogr.*, 2008, **223**, 399.

[24] C. Capillas, E. S. Tasci, G. de la Flor, D. Orobengoa, J. M. Perez-Mato and M.I. Aroyo, *Z. Kristallogr.*, 2011, **226,**186.

[25] M. Nespolo, G. Ferraris and H. Ohashi, *Acta Cryst. B*, 1999, **55**, 902,

[26] A. Simon and J. Ravez, *C. R. Chimie*, 2006, **9**, 1268.

[27] X. Kuang, F. Pan, J. Cao, C. Liang, M. R. Suchomel, F. Porcher and M. Allix, *Inorg. Chem.*, 2013, **52**, 13244.

[28] E. Banks and A. Goldstein, *Inorg. Chem.*, 1968, **7**, 966.

[29] R. S. Roth and J. Waring, *Res. Natl. Bur. Stand. A*, 1966, **70**, 281.

[30] O. Savborg and M. Lundberg, *Mater. Res. Bull.*, 1980, **15**, 1433.

Supporting Information
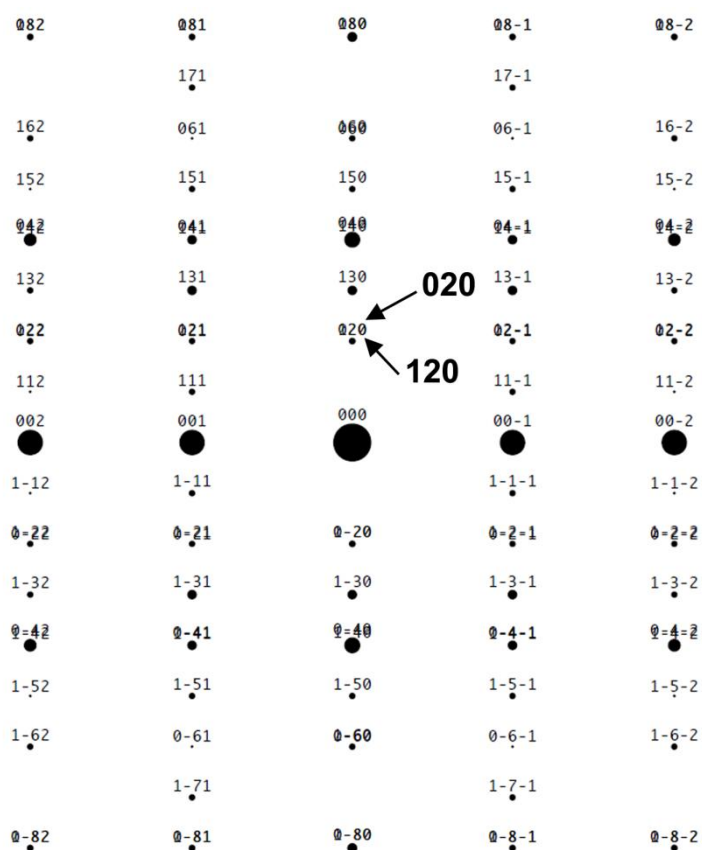
Fig. S1. Calculated selected area electron diffraction pattern of the [100] zone, using the final model as input. Overlap occurs at *k=2n* positions of the reflections of [100] and neighboring zones because of the small reciprocal *a** distance. All reflections with *k=2n+1* do not belong to the [100] zone itself, but are also visible here for the same reason as the overlapping *k=2n* reflections.
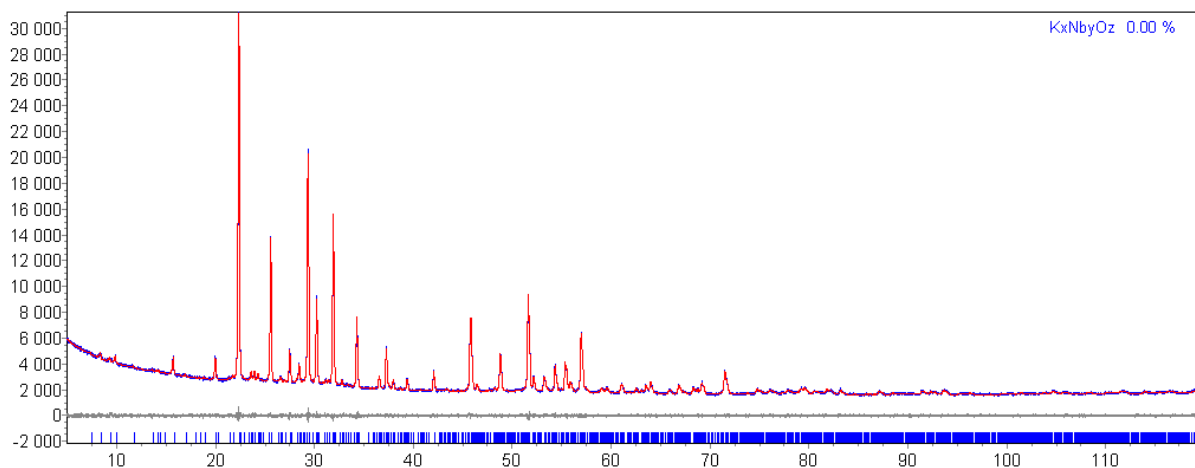
Fig. S2. Le Bail decomposition of PXRD profile (see description in the text). Experimental, calculated and difference curves are drawn with solid blue, red and grey lines, Bragg positions are marked with vertical blue bars.

Table S1

Atomic coordinates for $K_{6.4}Nb_{28.2}Ta_{8.1}O_{94.}$ (S.G. *Pbam*, $a = 37.461$ Å, $b = 12.471$ Å, $c = 3.954$ Å) as derived from transmission electron microscopy.

Atom	Wyckoff position	x/a	y/b	z/c
K1	2d	0.0000	0.5000	0.5000
K2°	4h	0.0558	0.2000	0.5000
K3	4h	0.1654	0.0126	0.5000
K4°	4h	0.2312	0.3207	0.5000
K5*	4h	0.95892	0.11645	0.5000
K6*	4h	0.71216	0.89315	0.5000
K7*	4h	0.62966	0.11454	0.5000
Nb1/Ta1	4g	0.9290	0.5563	0.0000
Nb2/Ta2	4g	0.8925	0.3166	0.0000
Nb3/Ta3	4g	0.9786	0.2908	0.0000
Nb4/Ta4	4g	0.8982	0.0586	0.0000
Nb5/Ta5	2a	0.0000	0.0000	0.0000
Nb6/Ta6	4g	0.8576	0.7781	0.0000
Nb7/Ta7	4g	0.2338	0.0665	0.0000
Nb8/Ta8	4g	0.1756	0.4907	0.0000
Nb9/Ta9	4g	0.1947	0.7633	0.0000
O1	4g	0.0920	0.2850	0.0000

O2	4g	0.9767	0.6228	0.0000
O3	4g	0.0582	0.5982	0.0000
O4	4g	0.8805	0.5120	0.0000
O5	4g	0.0695	0.8119	0.0000
O6	4g	0.8809	0.9144	0.0000
O7	4g	0.5022	0.3433	0.0000
O8	4g	0.9452	0.9801	0.0000
O9	4g	0.1884	0.1227	0.0000
O10	4g	0.2064	0.9144	0.0000
O11	4g	0.1404	0.8426	0.0000
O12	4g	0.1681	0.6383	0.0000
O13	4g	0.1738	0.3319	0.0000
O14	4g	0.2260	0.4681	0.0000
O15	4g	0.2458	0.7130	0.0000
O16	4h	0.8524	0.7908	0.5000
O17	4h	0.9268	0.5566	0.5000
O18	4h	0.8804	0.3572	0.5000
O19	4h	0.9711	0.2678	0.5000
O20	4h	0.9050	0.0665	0.5000
O21	2b	0.0000	0.0000	0.5000
O23	4h	0.2352	0.0798	0.5000
O24	4h	0.1685	0.4763	0.5000
O25	4h	0.1847	0.7781	0.5000

° K^+ in pentagonal channels, positions partially occupied by $Nb(Ta)^{5+}$

* K^+ in trigonal channels, occupation lower than 1

Table S2

Crystal data from refinement against combined X ray and neutron powder diffraction data.

$K_{6.4}Nb_{28.2}Ta_{8.1}O_{94}$	$\beta = 90°$
$M_r = 5822.65$	$\gamma = 90°$
Orthorhombic, *Pbam*	$V = 1850.54(63)$ Å^3
$a = 37.4676(90)$ Å	$Z = 1$
$b = 12.4934(30)$ Å	neutron radiation, $\lambda = 1.594$ Å
$c = 3.95333(15)$ Å	D_x, g cm^{-3} = 5.228
$\alpha = 90°$	

Fractional atomic coordinates and isotropic or equivalent isotropic displacement parameters (Å^2)

	x	y	z	U_{iso}*/U_{eq}	Occ. (<1)
K1/Nb1	0.449 (4)	0.344 (13)	0.5	2.42 (2)*	0.1486(55)/0.0132(55)
K2/Nb2	0.059 (2)	0.170 (6)	0.5	2.42 (2)*	0.7279(71)/0.2813(71)
K3	0.167 (3)	0.003 (8)	0.5	2.42 (2)*	0.4351(92)
K4/Nb4	0.226 (3)	0.332 (8)	0.5	2.42 (2)*	0.2884(92)/0.2804(90)
Nb1/Ta1	0.9300 (18)	0.573 (5)	0	2.42 (2)*	0.669(13)/0.331(13)
Nb2	0.8898 (12)	0.323 (3)	0	2.42 (2)*	1.0
Nb3/Ta3	0.9765 (16)	0.297 (6)	0	2.42 (2)*	0.776(13)/0.224(13)
Nb4/Ta4	0.903 (2)	0.067 (5)	0	2.42 (2)*	0.697(12)/0.303(12)
Nb5/Ta5	0	0	0	2.42 (2)*	0.604(17)/0.396(17)
Nb6/Ta6	0.8574 (19)	0.792 (6)	0	2.42 (2)*	0.670(10)/0.330(10)
Nb7/Ta7	0.2354 (19)	0.072 (5)	0	2.42 (2)*	0.705(13)/0.295(13)
Nb8/Ta8	0.1677 (12)	0.495 (4)	0	2.42 (2)*	0.639(11)/0.361(11)
Nb9/Ta9	0.1911 (18)	0.791 (6)	0	2.42 (2)*	0.714(35)/0.286(35)
O1	0.0970 (12)	0.291 (2)	0	2.42 (2)*	1.0
O2	0.9817 (7)	0.6092 (16)	0	2.42 (2)*	1.0
O3	0.0559 (5)	0.5794 (18)	0	2.42 (2)*	1.0
O4	0.8822 (5)	0.5011 (14)	0	2.42 (2)*	1.0
O5	0.0719 (5)	0.7850 (16)	0	2.42 (2)*	1.0
O6	0.8805 (7)	0.9275 (18)	0	2.42 (2)*	1.0
O7	0	0.160 (3)	0	2.42 (2)*	1.0
O8	0.9493 (6)	0.991 (2)	0	2.42 (2)*	1.0
O9	0.1918 (5)	0.1454 (16)	0	2.42 (2)*	1.0
O10	0.2071 (7)	0.934 (2)	0	2.42 (2)*	1.0
O11	0.1407 (6)	0.843 (2)	0	2.42 (2)*	1.0
O12	0.1666 (5)	0.6483 (15)	0	2.42 (2)*	1.0
O13	0.1687 (5)	0.3438 (15)	0	2.42 (2)*	1.0
O14	0.2195 (6)	0.4914 (19)	0	2.42 (2)*	1.0
O15	0.2629 (7)	0.207 (4)	0	2.42 (2)*	1.0

O16	0.8595 (12)	0.788 (3)	0.5	2.42 (2)*	1.0
O17	0.9297 (9)	0.578 (3)	0.5	2.42 (2)*	1.0
O18	0.8922 (11)	0.324 (5)	0.5	2.42 (2)*	1.0
O19	0.9774 (7)	0.3100 (15)	0.5	2.42 (2)*	1.0
O20	0.9001 (5)	0.0617 (19)	0.5	2.42 (2)*	1.0
O21	0	0	0.5	2.42 (2)*	1.0
O23	0.2374 (8)	0.074 (4)	0.5	2.42 (2)*	1.0
O24	0.1703 (7)	0.488 (2)	0.5	2.42 (2)*	1.0
O25	0.1918 (9)	0.784 (2)	0.5	2.42 (2)*	1.0